

# Localization Accuracy of Distributed Inverse Solutions for Electric and Magnetic Source Imaging of Interictal Epileptic Discharges in Patients with Focal Epilepsy

Marcel Heers · Rasheda A. Chowdhury · Tanguy Hedrich · François Dubeau · Jeffery A. Hall · Jean-Marc Lina · Christophe Grova · Eliane Kobayashi

Received: 22 September 2014/Accepted: 24 December 2014/Published online: 22 January 2015  
© Springer Science+Business Media New York 2015

**Abstract** Distributed inverse solutions aim to realistically reconstruct the origin of interictal epileptic discharges (IEDs) from noninvasively recorded electroencephalography (EEG) and magnetoencephalography (MEG) signals. Our aim was to compare the performance of different distributed inverse solutions in localizing IEDs: coherent maximum entropy on the mean (cMEM), hierarchical Bayesian implementations of independent identically distributed sources (IID, minimum norm prior) and spatially coherent sources (COH, spatial smoothness prior). Source maxima (i.e., the vertex with the maximum source amplitude) of IEDs in 14 EEG and 19 MEG studies from 15 patients with focal epilepsy were analyzed. We visually compared their concordance with intracranial EEG (iEEG) based on 17 cortical regions of interest and their spatial

dispersion around source maxima. Magnetic source imaging (MSI) maxima from cMEM were most often confirmed by iEEG (cMEM: 14/19, COH: 9/19, IID: 8/19 studies). COH electric source imaging (ESI) maxima co-localized best with iEEG (cMEM: 8/14, COH: 11/14, IID: 10/14 studies). In addition, cMEM was less spatially spread than COH and IID for ESI and MSI ( $p < 0.001$  Bonferroni-corrected post hoc  $t$  test). Highest positive predictive values for cortical regions with IEDs in iEEG could be obtained with cMEM for MSI and with COH for ESI. Additional realistic EEG/MEG simulations confirmed our findings. Accurate spatially extended sources, as found in cMEM (ESI and MSI) and COH (ESI) are desirable for source imaging of IEDs because this might influence surgical decision. Our simulations suggest that COH and IID overestimate the spatial extent of the generators compared to cMEM.

M. Heers (✉) · F. Dubeau · J. A. Hall · C. Grova · E. Kobayashi  
Department of Neurology and Neurosurgery, Montreal  
Neurological Institute, McGill University, 3801 University  
Street, Room 786, Montreal, QC H3A 2B4, Canada  
e-mail: marcel.heers@gmail.com

M. Heers  
Epilepsy Center, University Medical Center Freiburg, Freiburg,  
Germany

R. A. Chowdhury · T. Hedrich · C. Grova  
Multimodal Functional Imaging Laboratory, Biomedical  
Engineering Department, McGill University, Montreal, Canada

J.-M. Lina · C. Grova  
Physnum-Team, Centre de Recherches Mathématiques,  
Montreal, Canada

C. Grova  
Physics Department and PERFORM Centre, Concordia  
University, Montreal, Canada

**Keywords** Electroencephalography (EEG) · Electric source imaging (ESI) · Focal epilepsy · Intracranial EEG · Magnetoencephalography (MEG) · Magnetic source imaging (MSI)

## Introduction

Electric and magnetic source imaging (ESI and MSI) of interictal epileptic discharges (IEDs) aim to determine the origin of epileptic activity based on non-invasively recorded EEG and MEG signals. ESI and MSI are contributory in the pre-surgical evaluation and decision for surgery in patients with focal epilepsy. They are especially useful in guiding the implantation of intracranial EEG (iEEG) electrodes, with a crucial value in cryptogenic or non-lesional focal epilepsy patients (Brodbeck et al. 2011; De

Tiege et al. 2012; Megevand et al. 2014; Rikir et al. 2014; Sutherling et al. 2008). EEG and MEG are complementary in the detection of IEDs due to the different characteristics of electric and magnetic fields. MEG is able to capture tangentially oriented sources that are otherwise obscured by radial sources in scalp EEG signals. The unknown individual skull/brain conductivity ratios additionally limit the accuracy of ESI (Goldenholz et al. 2009; Hämäläinen 1992; Iwasaki et al. 2005).

So far most clinical studies for source imaging have been performed using equivalent current dipole (ECD) models (Knowlton et al. 2008; Sutherling et al. 2008; Wennberg and Cheyne 2014a, b). The most obvious limitation of ECDs is that they do not take into account the spatial extent of the epileptic source. Combined EEG/iEEG and MEG/iEEG studies have demonstrated that extended areas (at least 6–10 cm<sup>2</sup> for EEG and 4 cm<sup>2</sup> for MEG) of synchronously active cortex have to be involved to produce IEDs that can be recognized by surface recordings (Lantz et al. 2003; Mikuni et al. 1997; Oishi et al. 2002; Tao et al. 2005; von Ellenrieder et al. 2014a). Especially for extended areas of epileptic activity, ECD localizations can even be misleading (Kobayashi et al. 2005).

By now several different distributed inverse solutions are available to overcome the limitations of the ECD model. It remains unknown which of these methods is able to recover the spatial extent of the underlying generators and therefore which method performs best when localizing IEDs. Their performances have been investigated using realistic simulations and iEEG confirmed clinical data: in a comparison between the maximum entropy on the mean method (MEM) (Amblard et al. 2004) with low resolution electromagnetic tomography (LORETA) (Pascual-Marqui et al. 1994) and the minimum norm estimate (MNE) (Hämäläinen and Ilmoniemi 1994) using realistic simulations of EEG data, Grova et al. (2006) reported that LORETA and MEM performed well to accurately localize epileptic sources and their spatial extent. In this study the MEM method additionally showed greater stability compared to LORETA. For IEDs recorded by MEG, it has been suggested the usage of several distributed and beamforming inverse solutions in order to reach accurate localization (de Gooijer-van de Groep et al. 2013). Subdural iEEG validated the results of this study on data of patients with focal epilepsy.

In a different study from our group involving realistic simulations of IEDs for MEG data, Chowdhury et al. (2013) compared methods implemented within the MEM and the hierarchical Bayesian source imaging frameworks, showing that MEM was sensitive to different spatial extents of simulated sources. In this study, coherent MEM (cMEM) was compared with hierarchical Bayesian methods implemented using similar data driven parcellation and

local smoothness priors. Using extended sources ranging from 3 to 30 cm<sup>2</sup>, cMEM was found more sensitive to the spatial extent of the sources than independent identically distributed sources (IID, minimum norm prior) and spatially coherent sources (COH, spatial smoothness prior) hierarchical Bayesian methods [SPM8 implementation (Friston et al. 2008)].

As a continuation of this previous study, the objective of our current project was to compare the performance of cMEM, COH and IID in localizing IEDs from both EEG and MEG data with subsequent iEEG investigations in patients with focal epilepsy. Further evaluations on realistic simulations of EEG/MEG IEDs were added, in order to confirm some results suggested by the analysis of clinical data.

## Methods

### Ethics Aspects

This study was approved by the Montreal Neurological Institute Research Ethics Board and all patients signed a written informed consent prior to the study.

### Patients

Out of 97 patients who underwent combined EEG/MEG recordings at the Montreal Neurological Institute (MNI) between 2009 and 2012, we retrospectively included all 15 patients who underwent subsequent iEEG investigations at the MNI. Clinical details about the included patients are summarized in Table 1.

### EEG/MEG Data Acquisition

Simultaneous EEG/MEG recordings were acquired at the Montreal Neurological Institute, McGill University and at the Department of Psychology, Université de Montréal using two 275 channel CTF-MEG-systems (MISL, Vancouver, Canada) with a 56 channel EEG-cap with ceramic electrodes (Easy-cap, Herrsching, Germany). EEG electrodes were placed according to the 10/20 system, with additional electrodes according to the 10/10 system also covering the inferior temporal regions (F1, FPZ, F2, AF7, AF3, AFZ, AF4, AF8, FT9, FC5, FC3, FC1, FCZ, FC2, FC4, FC6, FT10, C1, C2, CP5, CP3, CP1, CPZ, CP2, CP4, CP6, P9, P1, P2, P10, PO7, PO3, POZ, PO4, PO8). Anatomical landmarks (nasion, left and right pre-auricular points), EEG electrodes position and scalp-points sampling the head shape were digitized prior to the EEG/MEG recordings using a Polhemus 3D localizer (Colchester, NH, USA). EEG/MEG signals were recorded with patients at

**Table 1** Patients' clinical characteristics

ID	MRI	Time span EEG/ MEG—iEEG (months)	Duration iEEG (days)	IED types telemetry	IED types MSI/ESI	No. IEDs MEG	No. IEDs EEG
1	Normal	1	7	RO	RO	16	110
2	R HME	3	8	RF	RF	16	32
3	R HME	3	8	RF	RF	42	N/A
4	Normal	8	12	RFT	RFT	478	119
5	Normal	4	12	LP	LP	8	16
6	R PMG	1	16	RTP, RFT	RFT	5	9
7	Normal	4	15	RF (RP)	RF	6	37
8	Normal	4	15	RF (RP)	RF	10	N/A
9	L extended subcortical heterotopia post	2	15	LTP	LTP	26	14
10	L extended subcortical heterotopia post	2	15	LTP	LTP	40	N/A
11	L PMG	7	16	LFT	LT	17	28
12	RF FCD	7	16	biF	RF	6	N/A
13	RF FCD	23	6	RF	RF	207	207
14	RF FCD	1	6	RF	RF	155	102
15	RF FCD	0	13	RTPO (T4, T6, P4, O2)	RTPO, RTO (MEG)	58	307
16	RF FCD	0	13	RTPO (T4, T6, P4, O2)	RTPO, RTO (MEG)	38	N/A
17	Normal	5	16	LFT	LF	18	36
18	Normal	4	9	LFT	LFT	240	426
19	Normal	9	18	LpT, RFT	RFT	48	24

FCD focal cortical dysplasia, L left, R right, F frontal lobe, HME hemimegalencephaly, ID study number, iEEG intracranial EEG, N/A not available, O occipital lobe, P parietal lobe, PMG polymicrogyria, post. posterior, T temporal lobe

rest in a supine position. The total duration depended on the patient's comfort and occurrence of clinical events (8–10 runs of 6 min). No filters were applied to the MEG recording and a hardware high pass filter of 0.03 Hz was used for the EEG. The sampling rate was either 1,200 and 2,400 Hz. Runs with head movements exceeding a maximum of 0.5 mm were discarded.

#### EEG/MEG Data Pre-processing and Evaluation

EEG and MEG data were bandpass filtered between 0.3 and 70 Hz after a DC-offset was removed from the EEG/MEG data, and 60 Hz notch filter was further applied. Based on visual evaluation bad EEG channels were removed and an average reference montage was created for the EEG.

EEG/MEG data were evaluated for presence of IEDs. IEDs were independently visually marked in EEG and MEG traces using DataEditor software (MISL, Vancouver, Canada) by two clinical neurophysiologists (M.H., E.K.). Only IEDs without co-occurring artifacts (muscle, eye movements, blinks or electrocardiographic artifacts) were selected for further evaluation. Each IED type marked was defined as a study. The evaluators were blind for iEEG

results during dataset marking, source imaging and evaluation of the source imaging results. In 15 patients, 14 EEG studies and 19 MEG studies were marked independently. Each IED type was defined as study, with  $N > 5$  samples (Mamelak et al. 2002).

#### Forward Model and EEG/MEG Data Processing

The anatomical MRI for source imaging consisted of a T1 W MPRAGE 1 mm isotropic 3D acquisition (192 sagittal slices,  $256 \times 256$  matrix, TE = 2.98 ms, TR = 2.3 s, flip angle adjusted according to AC-PC, acquired in a Siemens Tim Trio 3T scanner). The MRI was segmented in skin, skull and grey-white matter junction using BrainVISA-4.2.1 software (<http://brainvisa.info>) (Mangin et al. 1995) for each patient. A head mesh was computed from the outer surface of the head, and a cortical surface mesh (approximately 8,000 vertices) was tessellated from the grey-white matter interface. The MRI and the two meshes were imported in brainstorm software (<http://neuroimage.usc.edu/brainstorm>) (Tadel et al. 2011), where individual three surfaces adapted for Boundary Element Models (BEM) were reconstructed (inner skull, outer skull and head). A 1-layer BEM (conductivity: 0.33

S/m) was considered to estimate the MEG forward model, whereas a 3-shell BEM (conductivity: 0.33, 0.165, 0.33 S/m; ratio: 1/20) (Chen et al. 2010; Goncalves et al. 2003) was considered for EEG. BEM models were estimated using OpenMEG method (Gramfort et al. 2010). Epochs (400 ms duration) containing every IED marked in EEG/MEG and a 2 s baseline were down-sampled to 600 Hz and imported into brainstorm software. The anatomical MRI and the segmentations were co-registered with the EEG/MEG data using the three fiducial landmarks and the headshape recorded with a Polhemus system prior to the EEG/MEG recording.

#### *Inverse Modeling Using the cMEM, COH and IID*

Source imaging was performed on averaged IEDs for patients with more than 10 markers per study (MSI: 14 studies, ESI: 13 studies) and single IED source imaging for patients with less than 10 markers (MSI: 5 studies, ESI: 1 study). For IEDs occurring across multiple runs, the source imaging findings of the averaged IEDs for each run were averaged (thus in source space and not on signal) over multiple runs. For single IEDs in different runs, source imaging was performed first and the findings were averaged in the source space over multiple runs. The idea of this approach was to find a systematic trade-off between maximal signal-to-noise ratio for source imaging (Bast et al. 2004) and the inability to correct, at the sensor space, MEG signal for movements between 6 min runs.

The source space model was restricted to the grey-white matter tessellated surface. All source localizations were considered at the main peak of the IED, and therefore eventual propagations were not taken into account.

Every source localization approach consists in solving an ill-posed inverse problem (Baillet et al. 2001). Therefore, some a priori knowledge should be incorporated within a regularization framework in order to estimate a unique solution. In the proposed study, we will compare three localization methods previously evaluated on simulated data (Chowdhury et al. 2013).

#### *Source Localization Within the MEM Framework*

The MEM framework has been validated as a source localization technique able to recover the spatial extent of the underlying sources (Chowdhury et al. 2013; Grova et al. 2006). MEM offers an efficient framework to incorporate prior knowledge in the resolution of the inverse problem (Amblard et al. 2004). In our current implementation of MEM, we assume brain activity to be modeled by cortical parcels. We proposed a data-driven parcellation (DDP) to cluster the whole cortical surface into K non-overlapping parcels, as originally proposed by Lapalme

et al. (2006). DDP consists in using partial information from the available data in order to guide this spatial clustering. The key aspect of DDP lies in the pre-localization of the sources of brain activity using the multivariate source pre-localization (MSP) method (Mattout et al. 2005). MSP is a projection method that estimates a coefficient, which characterizes the possible contribution of each dipolar source to the data. DDP in K parcels is then obtained using a region-growing algorithm around the local maxima of the MSP map. In the MEM reference model, a hidden variable is associated to each parcel in order to model the probability of the parcel to be active (probability initialized using the MSP coefficients).

In summary, thanks to such a DDP, MEM provides an interesting framework allowing switching off the parcels that do not contribute to the solution, while preserving the ability to create a contrast of current intensities within the active parcels. We demonstrated that the use of such a parcellation model is the key idea in order to provide a method sensitive to the spatial extent of the sources (Chowdhury et al. 2013). In this study, we will use the method entitled coherent MEM (cMEM), which further imposes a spatial smoothness constraint within each parcel (see Chowdhury et al. 2013 for further details). This implementation of cMEM algorithm is available in brain-storm software and a tutorial describing its use has been created: <http://neuroimage.usc.edu/brainstorm/Tutorials/TutBEst>.

#### *Source Localization Within the Hierarchical Bayesian Framework*

Solving the MEG inverse problem within the hierarchical Bayesian framework offers the advantage of accommodating multiple priors and proposes inference techniques to select the most likely combination of priors using model selection approaches (Friston et al. 2008).

Hierarchical Bayesian model allows integrating uncertainties at different levels, modeling the covariance in each level as a linear combination of covariance components. The different levels are the sensor noise level and the source noise level. The hyper-parameters are then estimated from the data using a Restricted Maximum Likelihood algorithm, selecting the most relevant linear combination of covariance components (Friston et al. 2002). In this study, we will compare cMEM with two standard source reconstruction methods implemented in SPM8 software package (<http://www.fil.ion.ucl.ac.uk/spm/>) (Friston et al. 2008):

- (a) *Independent and identically distributed model (IID)*  
a single source covariance component encoding identically and independently distributed sources

(i.e. identity matrix) is assumed. This method provides thus a minimum energy solution, similar to the one originally proposed by Hämäläinen and Ilmoniemi (1994).

- (b) *Spatially coherent sources (COH)* This method provides a solution that is spatially smooth, similar to LORETA (Pascual-Marqui et al. 1994). The model is composed of two spatial components modeling respectively IID sources (identity matrix) and spatially coherent sources (spatial smoothness constraint). COH is an interesting method providing a balance between a minimum norm and a LORETA-like solution, while the balance between these two priors is tuned from the data, using Restricted Maximum Likelihood estimation.

Whereas IID could be considered as the most standard and widely used distributed source localization method (minimum norm estimate), COH provides a very interesting alternative, showing good performance in the presence of spatially extended sources is demonstrated in Chowdhury et al. (2013). Therefore we chose these two methods for our comparison with cMEM on clinical data.

#### IEEG

IEEG investigations for presurgical evaluation were performed at the Montreal Neurological Institute subsequently to the ESI/MSI recordings in 15 patients included in this study. In 14 of these patients 5–11 depth electrodes (with

8–10 contacts each) to target brain areas suspected to be involved in the epileptic focus were implanted. In one patient a subdural electrode grid with  $8 \times 8$  contacts was implanted.

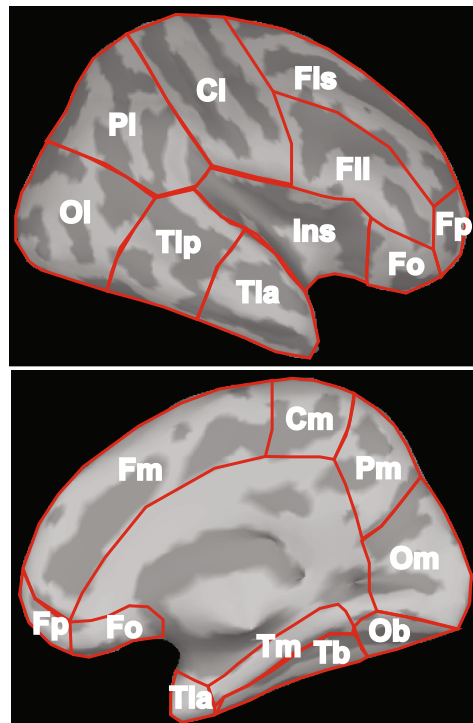
#### Comparison of ESI/MSI with iEEG

ESI/MSI results for each study were compared qualitatively with clinical iEEG reports of an expert neurophysiologist's (F.D.) evaluation of the signals and of post-implantation MRI/computerized tomography (CT).

For this assessment each patient's cortical surface was visually divided into 17 clinically relevant regions of interest (ROIs) as illustrated in Fig. 1 expanding the 10 ROIs used by de Gooijer-van de Groep et al. (2013). For comparison with iEEG we defined the vertex with the maximum source amplitude as *primary source maxima* of ESI or MSI. The spatial extent was not considered in this comparison. Primary topographical source maxima were compared to iEEG findings according to the following criteria:

- *Confirmed by iEEG* IEDs were reported from the iEEG recordings for contacts in the same ROI as the source maximum of ESI/MSI.
- *Not covered by iEEG* No iEEG contacts were implanted in the ROI where the ESI/MSI source maxima were localized.
- *ESI/MSI contralateral* Source maxima were found in the hemisphere contralateral to the magnetic field

**Fig. 1** Seventeen regions of interest (ROIs) expanding the 10 ROIs applied by de Gooijer-van de Groep et al. (2013) were used for the visual comparison of ESI/MSI maxima with IEDs recorded by iEEG



Cl	= Central, lateral
Cm	= Central, mesial
Fli	= Frontal, lateral inferior
Fls	= Frontal, lateral superior
Fm	= Frontal, mesial
Fo	= Frontal, orbital
Fp	= Frontal, polar
Ins	= Insula
Ob	= Occipital, basal
OI	= Occipital, lateral
Om	= Occipital, mesial
Pl	= Parietal, lateral
Pm	= Parietal, mesial
Tb	= Temporal, basal
Tla	= Temporal, lateral anterior
Tlp	= Temporal, lateral posterior
Tm	= Temporal, mesial

topography zero line (MSI) or to the maximum negative electric potential (ESI) in the sensor space, where there were no IEDs in iEEG. This criterion was introduced to identify sources that are likely to be spurious and an error resulting from the applied inverse model.

We did not observe ESI/MSI source maxima within ROIs that were covered by iEEG electrodes, but for which no IEDs were recorded by iEEG. Thus we did not add such a category in the comparison of ESI/MSI with iEEG.

In addition to primary source maxima of ESI/MSI, we also evaluated secondary source maxima for each inverse model in each patient. The secondary source maxima of ESI/MSI maps were defined as the local source maxima showing the source maximum of the second largest intensity. To be considered as a secondary source maximum, this local maximum had to be (1) localized in a different ROI than the primary source maximum and (2) with an amplitude >50 % of the maximum amplitude. Whenever present, a secondary source maximum was evaluated using the same criteria as used to evaluate the primary source maximum. Otherwise it was stated that there was no secondary maximum. All visualizations for these comparisons and all figures illustrating source imaging results in the manuscript were created using *brainstorm* software (Tadel et al. 2011).

#### *Positive Predictive Value and Sensitivity*

To compare source imaging accuracy for the different inverse models, we calculated the positive predictive values (PPVs) and sensitivities of the primary source maxima to identify brain regions that contained IEDs according to iEEG recordings, following the approach by de Gooijer-van de Groep et al. (2013). Comparisons between primary source maxima and iEEG were defined as true positive, if they co-localized with ROIs that produced IEDs according to iEEG. The comparison was defined as true negative, if there was no source maximum in a specific ROI but an iEEG electrode and no IEDs were recorded with the contacts of this respective iEEG electrode. The comparison was counted as false negative, when IEDs were present according to iEEG in the respective ROI, but there was no source maximum in this ROI. Whenever there was a source maximum in one ROI, but there were no IEDs recorded by iEEG within the same ROI, the comparison was counted as false positive. Sensitivities and PPVs were calculated over all studies according to the following formulas:

#### *Sensitivity (%)*

$$= \frac{\text{Number of true positives}}{\text{Number of true positives} + \text{number of false negatives}} \times 100$$

#### *Positive predictive value (%)*

$$= \frac{\text{Number of true positives}}{\text{Number of true positives} + \text{number of false positives}} \times 100$$

Sensitivity values have to be treated with caution, as they not only depend on the localization accuracy of the inverse solution, but also on characteristics of EEG and MEG for detection of IEDs.

In addition to sensitivities and positive predictive values for the evaluation of single inverse methods, we calculated positive predictive values and sensitivities for different combinations of concordances between findings of all three inverse methods. This was done to study whether combining several inverse methods improves the concordance with iEEG findings as reported by de Gooijer-van de Groep et al. (2013).

#### *Comparison of Spatial Dispersion (SD) with and without Gold Standard ( $SD_{gs}$ ; $SD_{ngs}$ )*

In addition to the localization accuracy of the source maxima, we evaluated the spatial distribution of the sources using a SD metric. SD is a measure of both the spatial spread of the estimated source distribution around the true source location and the localization error between the estimated source distribution and the true source location. This metric has been introduced for the analysis of spatial resolution of source imaging technique (Molins et al. 2008).

Let us denote by  $\hat{J}$  the solution of a source localization method. Then,  $\hat{J}_i$  represents the amplitude of the current density distribution estimated for a dipolar source  $i$  on the cortical surface at the main peak of the IED. To measure SD for this solution, we weighted the amplitude of all the  $p$  cortical sources by their minimum distance from a reference  $\Theta$  using the following formula:

$$SD = \sqrt{\frac{\sum_{i=1}^p (\min_{j \in \Theta}(D_{ij}) \hat{J}_i^2)}{\sum_{i=1}^p \hat{J}_i^2}}$$

where  $\min_{j \in \Theta}(D_{ij})$  provides the minimum distance between the source  $i$  and the closest dipolar source of the reference  $\Theta$ , and this minimum distance is zero whenever the source  $i$  belongs to the reference. SD values close to zero means there is no active source outside the reference source location. A high value of SD means there are spurious sources far away from the reference source that are contributing to the estimated solution or the reconstructed source map is spatially spread around the reference.

When localizing clinical data, there is no Gold Standard on the spatial extent of the source. Therefore, we adapted the definition of SD for clinical data, which will be denoted

as  $SD_{ngs}$ . In  $SD_{ngs}$ , the reference  $\Theta$  has been defined as a set of cortical sources exhibiting local maxima of the reconstructed source distribution. Then, we weight the amplitude of the estimated source  $i$  with the distance to the closest local source maxima. Local source maxima were determined based on ESI/MSI amplitude maps and defined using the following constraints:

- The amplitude of the local source maxima should be at least 80 % of the maximum amplitude.
- The local source maxima should not be closer than 3 cm from a local source maximum with higher amplitude (3 cm Euclidean distance)

To statistically compare SD values obtained using cMEM, COH and IID, we first used a one-way ANOVA to test for significant differences between the inverse solutions and subsequent two-tailed paired sample  $t$  test.

#### Validation Using Simulations

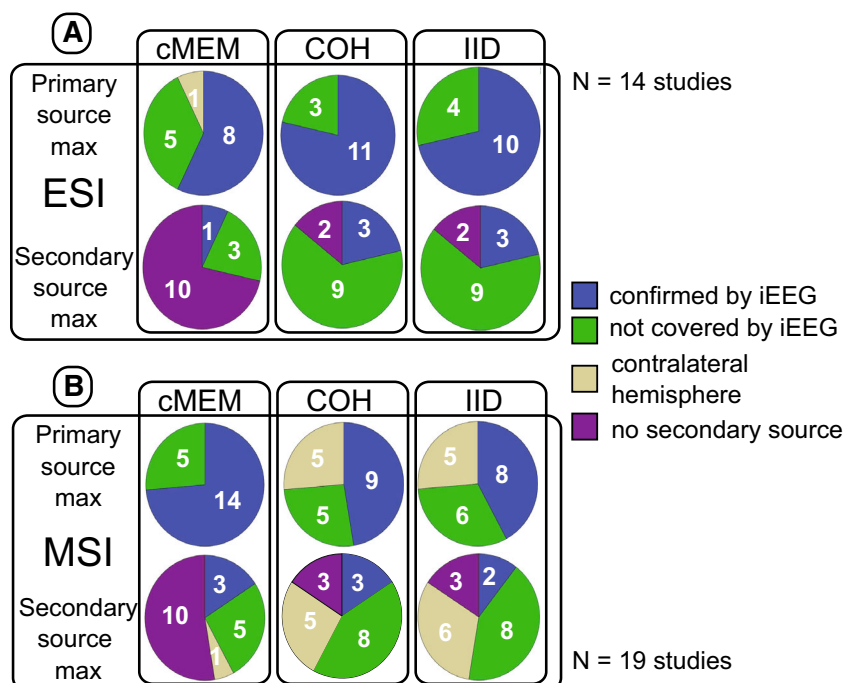
To further understand our clinical findings characterized by SD values, we studied the behavior of such a metric in a fully controlled environment using realistic simulations of 50 neocortical IEDs. Simulations were generated following the same methodology as described in Chowdhury et al. (2013). These sources were selected by positioning seed points randomly on the neocortical surface of the segmented grey-white matter junction. Spatially extended generators were simulated cycling systematically through three to five neighborhood orders of vertices for all 50 sources along the cortical surface ( $\sim 2\text{--}16\text{ cm}^2$ ). The

spatial extent of each generator was thus obtained by region growing around the seeds following the cortical gyration. Time courses of epileptic spikes were simulated using three gamma-functions applied to the sources of the simulated generator, and noise-free EEG/MEG signals were then constructed by applying the respective forward model to these theoretical current densities. Note that only the simulated signal around the first peak of the simulated IED was taken into account. Realistic EEG/MEG noise was acquired in a patient with focal epilepsy. An epoch free of IEDs and eye movement artifacts was selected. From this background activity 128 epochs of 700 ms length were chosen. The amplitude of the background activity trials was scaled to ensure a signal-to-background ratio of 1 (0 dB) for most superficial sources, when using reference source amplitude of 9.5 nAm for each dipolar source along a patch of  $6\text{ cm}^2$ . From these 128 epochs 20 were randomly selected and averaged to simulate the averaging of IEDs. Finally, they were added to the simulated noise-free signal.

When localizing simulated data, the Gold Standard on the spatial extent of the source is fully known. In such cases, we will denote the measure of SD as  $SD_{gs}$  and the reference  $\Theta$  will be the set of cortical sources inside the simulated patch. ESI and MSI on these simulations were performed using cMEM, IID and COH. We estimated both  $SD_{gs}$  and  $SD_{ngs}$  for the sources reconstructed using cMEM, IID and COH to further characterize the SD metric when applied on clinical data.

As for the clinical data, we used one-way ANOVA and post hoc paired sample  $t$ -test to compare and test for statistical SD differences between cMEM, COH and IID.

**Fig. 2** Pie charts illustrating the comparison of primary ESI/MSI source maxima with iEEG findings. **A** There is an overall good agreement of primary ESI maxima obtained from all three inverse methods with iEEG findings. To note, there were almost no secondary source maxima found for cMEM and many secondary source maxima for COH and IID remained unconfirmed by iEEG. **B** The best agreement with iEEG findings was found for cMEM MSI results. Similarly to ESI observations, cMEM most often did not reveal secondary sources. When identified with COH and IID, secondary sources were most often not confirmed by iEEG



## Results

### Source Maxima and Comparison with iEEG

#### *MSI—iEEG*

In most MSI studies (14/19) iEEG confirmed the primary cMEM source maxima, compared to a worse performance from COH (9/19) and IID (8/19). Non-concordant results were found for all three methods. In some studies, the primary source maxima using COH and IID were found

over the contralateral hemisphere, in disagreement with the magnetic field topography (COH: 5/19, IID: 6/19). This was not the case for cMEM primary source maxima (Figs. 2, 3, 4; Table 2). IEEG electrodes did not cover a minority of primary MSI source maxima (cMEM 5/19, COH 5/19, IID 6/19).

No secondary MSI maxima were found for cMEM sources in 10/19 studies (COH and IID: 3/19). In 5/19 studies iEEG with secondary MSI cMEM maxima, these were confirmed with iEEG (COH: 3/19 and IID: 2/19). COH and IID MSI findings exhibited more frequently

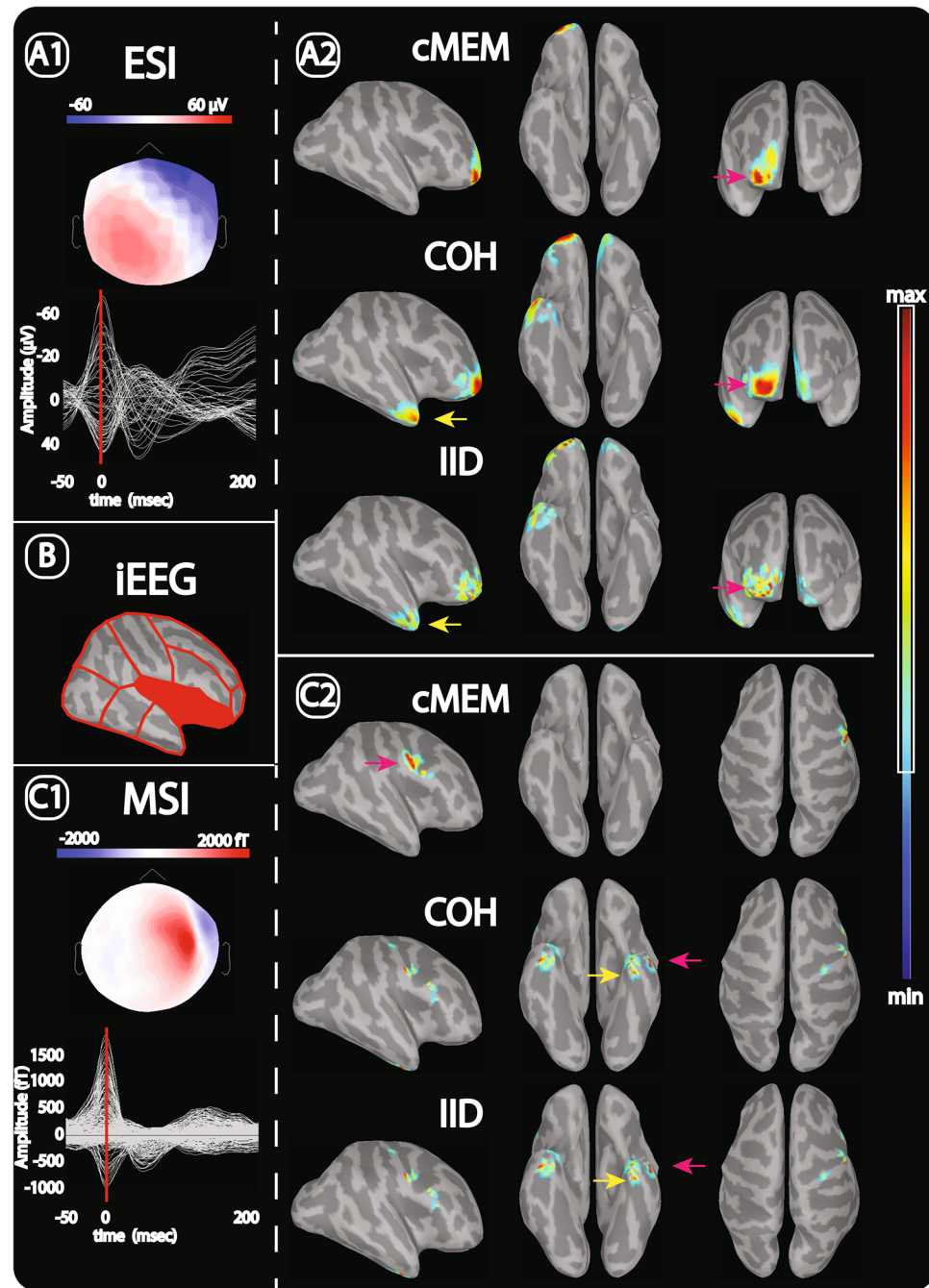


**Fig. 3** (Study 2) Comparison of ESI and MSI results obtained with cMEM, COH and IID with iEEG clinical data, in a patient with hemimegalencephaly. **A** Electric source imaging (ESI): left **A1** topographic map of the averaged IEDs (*red line* indicates IED peak) used for ESI, right **A2** ESI findings for cMEM (first row), COH (second row) and IID (third row). **B** Cortical regions of interest (ROIs) represented over the surface of a T1 MRI surface in standard space. The *red lines* denote boundaries between the different ROIs (from Fig. 1). ROIs within which IEDs have been found in iEEG data are *red filled*. **C** Magnetic source imaging (MSI): left **C1** topographic map of the averaged IEDs (*red line* indicates IED peak) used for MSI, right **C2** MSI findings for cMEM (first row), COH (second row) and IID (third row). Primary source maxima (i.e. vertex with the maximum source amplitude) are indicated with *pink arrows*, secondary source maxima are marked with *yellow arrows* for ESI and MSI. All ESI and MSI results displayed over the cortical surface are thresholded at 30 % of the maximum amplitude. ESI and MSI were performed on IEDs independently marked in EEG and MEG traces. **A2** The primary ESI source maximum not concordant with iEEG was found for cMEM, COH, IID involving the right frontal polar region. iEEG recorded orbito-frontal IEDs. Secondary source maxima were seen only for COH and IID, involving the lateral aspect of the right temporal pole (not covered by iEEG). **B** IEDs recorded with iEEG over the right insula and right orbitofrontal area. **C2** In MSI, the primary source maximum was seen over the inferior aspect of the precentral sulcus, with a clear distinct source in cMEM confirmed by iEEG recordings. Primary source maxima for COH and IID were found over the left anterior lateral temporal lobe not in agreement with zero line of the MEG field topography. Primary source maxima are defined as the vertex with highest total source amplitude. Because of the localization over the contralateral hemisphere of the COH and IID primary source maxima compared to the field topography, these sources were counted in the group of contralateral sources that are likely to be spurious. This area was also not covered by iEEG. No secondary source maxima occurred for cMEM. Secondary source maxima for COH and IID were localized over the left mesial temporal lobe. They were counted as separate source, because according to our definition secondary sources were recognized as separate source, whenever the first vertex occurred in a different ROI compared to the primary source maximum while decreasing the amplitude threshold. For COH and IID there was also a source in concordance with the cMEM source and iEEG findings. The amplitude of these sources was however lower than the primary and secondary source maxima (Color figure online)

secondary maxima, which were either not confirmed by iEEG (COH: 8/19, IID: 8/19) or localized over the contralateral hemisphere (COH: 5/19, IID: 6/19) (Figs. 4, 5). For cMEM secondary MSI maxima were not confirmed by iEEG in 5/19 studies and in only 1/19 studies it localized to the contralateral hemisphere.

In the evaluation of single inverse methods, cMEM showed the largest PPV and sensitivity values followed by COH and IID (Table 3). Combining either COH or IID with cMEM resulted in the largest increase in PPVs. For cMEM MSI findings, this also resulted in a drop of sensitivities from 40 to 25 %.

For neocortical cases we did not observe any obvious relationship between the accuracy of MSI and a specific epilepsy syndrome or the topography of IEDs recorded by iEEG. MSI findings were never concordant with mesial temporal lobe IEDs recorded with iEEG, and this is

expected. We recognize that we several times identified orbitofrontal primary source maxima using MSI that were confirmed by iEEG (studies 7, 8 and 11). This may be explained by the tangential orientation of orbitofrontal generators of IEDs, for which the signal to noise ratio in MEG is high (Goldenholz et al. 2009).

#### ESI—iEEG

In the majority of ESI studies the primary source maxima for cMEM (8/14), COH (11/14) and IID (10/14) were confirmed by iEEG (Fig. 2). For one ESI study, we observed a cMEM source maximum that localized to the interhemispheric border of the contralateral hemisphere compared to the electric field topography directly next to the frontal interhemispheric fissure (Fig. 6). Similar to MSI, a minority of primary ESI maxima could not be confirmed by iEEG for all three inverse solutions (cMEM: 5/14, COH: 3/14, IID: 4/14).

No secondary source maxima were detected for cMEM in 10/14 studies, while most studies showed secondary source maxima in COH and IID. These however, were most often (COH: 9/14, IID: 9/14) not confirmed by iEEG (Figs. 2, 4, 5). No secondary ESI maxima occurred over the contralateral hemisphere for any of the inverse methods.

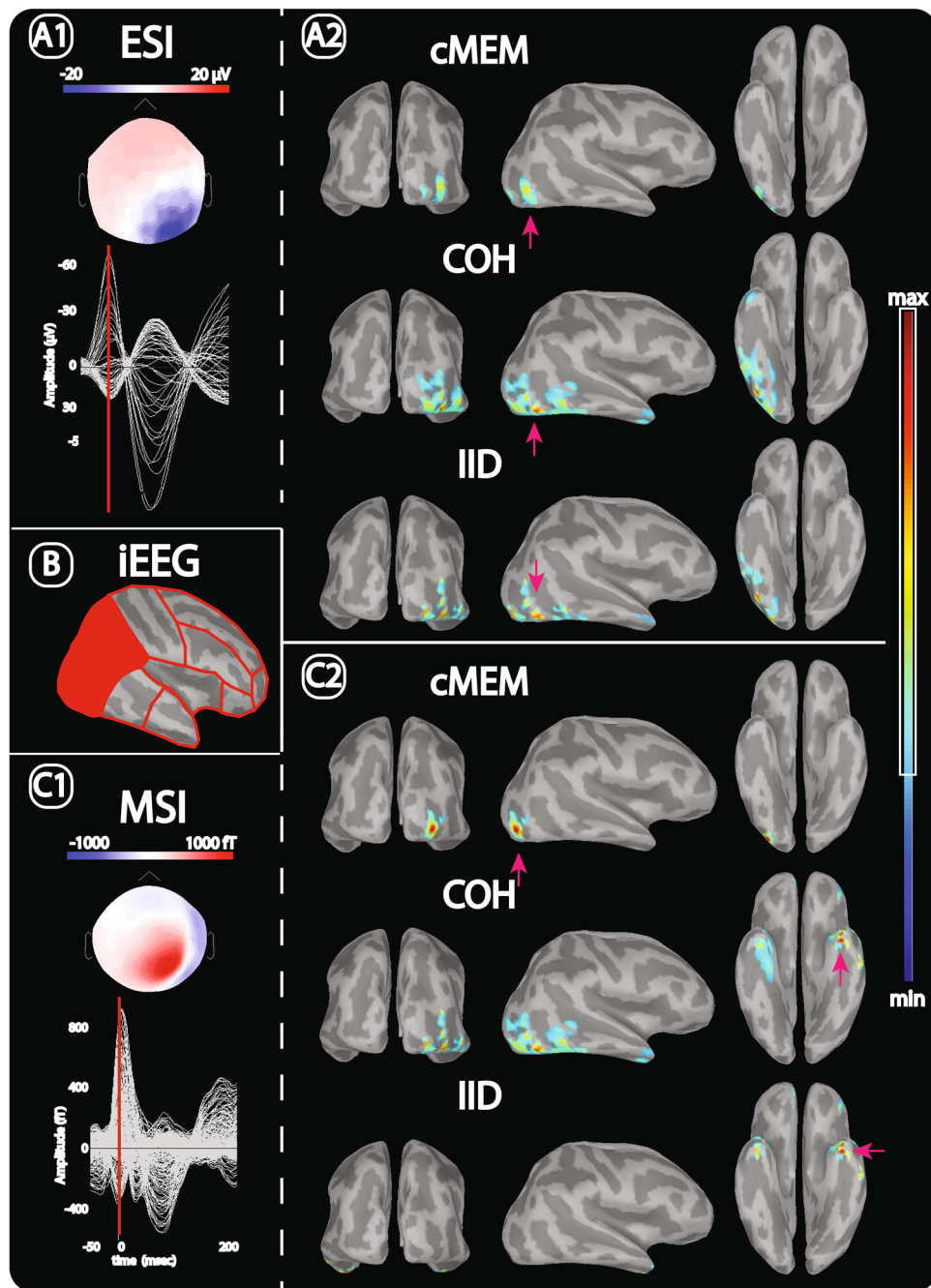
PPVs were highest for COH, followed by IID and cMEM (Table 3). Combining concordant inverse methods increased PPVs particular when involving cMEM. As in MSI the increase in the PPV was also for ESI at the cost of a remarkably decreased sensitivity.

Similar to MSI we could not identify any convincing relation between the accuracy of ESI and a specific etiology of the epilepsy syndrome or the localization of the IEDs recorded in iEEG for neocortical epilepsy. As for MSI there was no concordance between ESI and mesial temporal IEDs recorded in iEEG. Again similar to MSI we did not find that any of the used inverse solutions performed better or worse for a specific localization.

#### SD and Visual Evaluation of Spatial Spread of ESI/MSI in Epilepsy Patients

One-way ANOVA identified a difference of SD for cMEM, COH and IID for MSI ( $F: 28.22, p < 0.001$ ) and ESI ( $F: 22.87, p < 0.001$ ). Post-hoc two-tailed and Bonferroni-corrected t-test proved that cMEM sources are significantly less spatially spread than COH and IID sources ( $p < 0.001$ ) for ESI and MSI (both  $p < 0.001$ ). Thus we believe that cMEM ESI and MSI findings are much more sensitive to the spatial extent of the cortical generator of epileptic activity, when compared to IID or COH (e.g. Figs. 5, 7).

In summary we found in the clinical evaluation of ESI and MSI using cMEM, COH and IID that their primary



source maxima were most often confirmed by iEEG. For COH and IID secondary source maxima were often not concordant with iEEG and they were found over the contralateral hemisphere. Secondary source maxima occurred less frequently for cMEM compared to COH and IID. As the SD proves that cMEM sources are significantly less spatially spread around local maxima than COH and IID sources for ESI and MSI, we believe that cMEM allows recovering the spatial extent of the cortical generators more accurately.

Because it is difficult to validate this assumption using depth EEG recordings, we tested the performance of SD for

cMEM, COH and IID in a fully controlled realistic simulation framework. In addition this allows us to verify that SD is suitable to evaluate spatial spread of ESI and MSI findings caused by different inverse solutions.

#### Realistic Simulations

##### $SD_{gs}$ and $SD_{ngs}$

We found very similar results for the  $SD_{gs}$  and  $SD_{ngs}$  of cMEM, IID and COH. This was true for ESI and MSI and for different spatial extents (Fig. 8). It means that the

**Fig. 4** (Study 15) Comparison of ESI and MSI results obtained with cMEM, COH and IID with iEEG clinical data, in a patient with focal cortical dysplasia. **A** Electric source imaging (ESI): *left A1* topographic map of the averaged IEDs (*red line* indicates IED peak) used for ESI, *right A2* ESI findings for cMEM (*first row*), COH (*second row*) and IID (*third row*). **B** Cortical regions of interest (ROIs) represented over the surface of a T1 MRI surface in standard space. The *red lines* denote boundaries between the different ROIs (from Fig. 1). ROIs within which IEDs have been found in iEEG data are *red filled*. **C** Magnetic source imaging (MSI): *left C1* topographic map of the averaged IEDs (*red line* indicates IED peak) used for MSI, *right C2* MSI findings for cMEM (*first row*), COH (*second row*) and IID (*third row*). Primary source maxima (i.e. vertex with the maximum source amplitude) are indicated with *pink arrows*, secondary source maxima are marked with *yellow arrows* for ESI and MSI. All ESI and MSI results displayed over the cortical surface are thresholded at 30 % of the maximum amplitude. ESI and MSI were performed on IEDs independently marked in EEG and MEG traces. **A2** Primary ESI source maxima for cMEM, COH and IID were found in the lateral inferior aspects of the right occipital pole (source confirmed by iEEG). **B** iEEG recorded IEDs over the right lateral parietal and occipital lobes. **C2** In MSI, primary source maximum was found in the same topography as ESI (described above) for cMEM, whereas COH and IID primary sources were seen in the basal left temporal pole (not covered with iEEG electrodes). Secondary sources for COH were seen on the left temporal lateral anterior (not shown on figure) and another source was seen in the exact location as ESI primary source confirmed by iEEG. For IID, secondary sources were left temporal lateral anterior (not shown on figure). In this patient, for whom the clinical hypothesis was very clear resulting in an iEEG investigation optimized and targeting the right posterior quadrant region, results in the two modalities (i.e., EEG and MEG) illustrate well the effect that the choice of different inverse solutions (i.e., cMEM, COH or IID) might have in ESI and MSI (Color figure online)

choice of local source maxima as reference  $\Theta$  in the SD estimation is reliable for the clinical data localization, since it provides similar trends than when choosing the gold standard as the reference  $\Theta$  for simulated data. Therefore, it justifies applying SD on clinical epilepsy data without knowing the exact extent of the underlying sources. In agreement with findings from the clinical data, the comparison between cMEM, IID and COH revealed significantly lower spatial dispersion for cMEM (around the true source  $SD_{gs}$ : ESI: F: 153.84, MSI: F: 77.93, both  $p < 0.001$ ; around local maxima  $SD_{ngs}$ : ESI: F: 88.5, MSI: F: 167.74, both  $p < 0.001$ ) than for IID and COH. This was true for ESI as well as for MSI data. In summary, these simulations are confirming our clinical data that cMEM was less susceptible to overestimation of the spatial extent around the true source and to the generation of distant spurious activity than IID and COH.

## Discussion

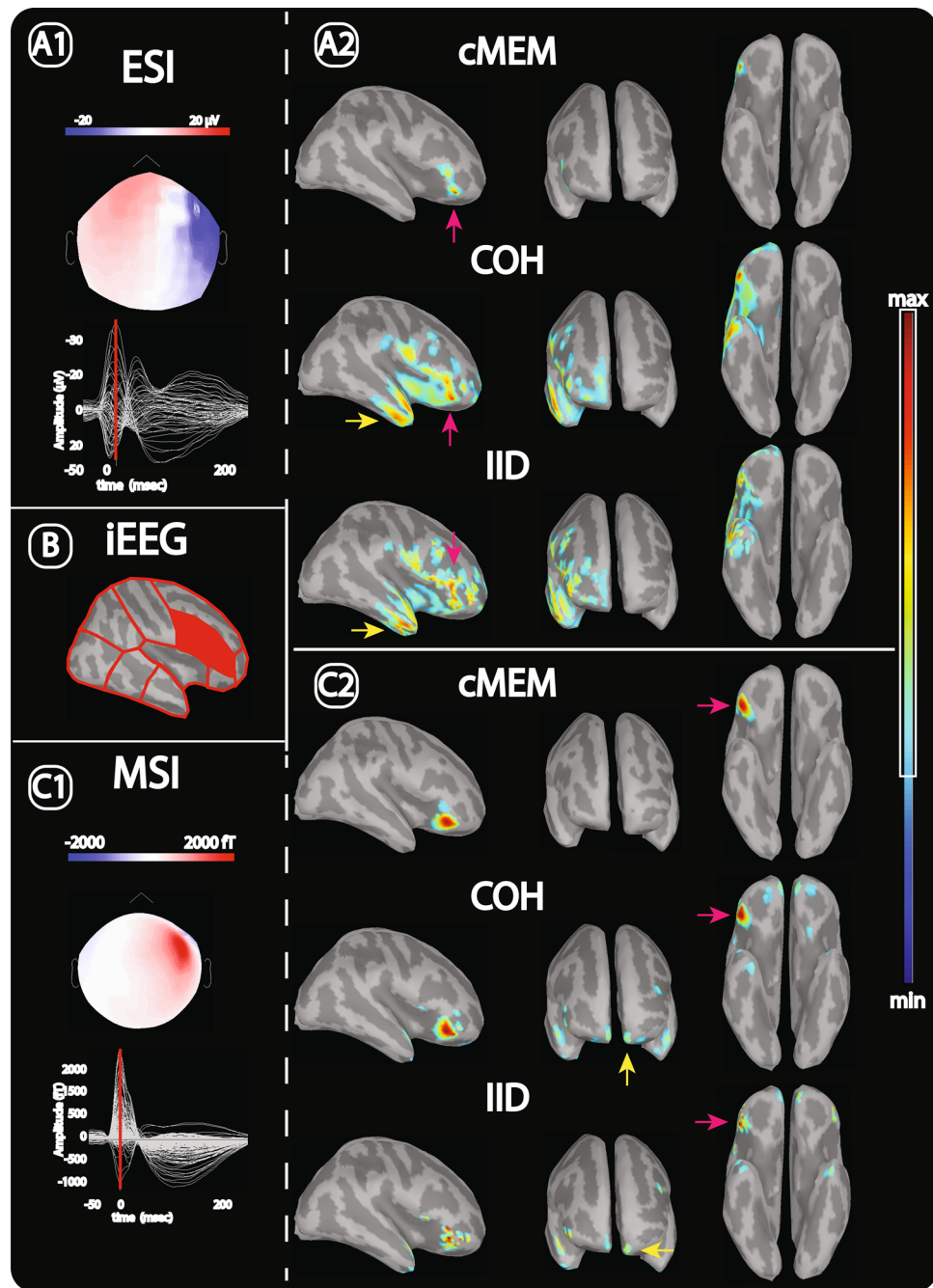
This is the first study that systematically evaluates ESI and MSI from simultaneous EEG/MEG recordings using different distributed inverse solutions in patients with focal epilepsy. We showed on ESI and MSI of IEDs that iEEG

**Table 2** Comparison of primary source maxima with different types of IEDs recorded by iEEG

No.	MSI			ESI			iEEG			
	cMEM	COH	IID	cMEM ESI	COH ESI	IID ESI	iEEG I	iEEG II	iEEG III	iEEG IV
1	<i>ROb</i>	<b>RTla</b>	<b>RTla</b>	<i>ROl</i>	<i>ROl</i>	<i>ROl</i>	<b>ROb</b>	<b>ROl</b>	<b>RTm</b>	<b>RPI</b>
2	<b>RCI</b>	<i>LTLa</i>	<i>LTLa</i>	<b>RFP</b>	<b>RFP</b>	<b>RFP</b>	<b>RFO</b>	<b>RIns</b>	<b>LTm</b>	
3	<b>RFP</b>	<i>LTLa</i>	<i>LTLa</i>	N/A	N/A	N/A	<b>RFO</b>	<b>RIns</b>	<b>LTm</b>	
4	<i>RFli</i>									
5	<b>LTLa</b>	<b>RTla</b>	<b>RTla</b>	<i>LCl</i>	<i>LCl</i>	<b>LTLa</b>	<i>LCl</i>	<b>RTP</b>		
6	<i>RTla</i>	<i>RTla</i>	<i>RTla</i>	<b>RFli</b>	<i>RTla</i>	<i>RTla</i>	<i>RTla</i>	<i>RIns</i>		
7	<b>RFO</b>	<b>RFP</b>	<b>RFP</b>	<i>LFls</i>	<b>ROI</b>	<b>ROI</b>	<b>RFO</b>	<b>RH</b>	<b>RLC</b>	<b>RFLs</b>
8	<b>RFO</b>	<b>RFP</b>	<b>RFP</b>	N/A	N/A	N/A	<b>RFO</b>	<b>RH</b>	<b>RLC</b>	<b>RFLs</b>
9	<i>LTLp</i>	<i>LTLp</i>	<i>LTLp</i>	<b>LIns</b>	<b>LOI</b>	<b>LOI</b>	<i>LTLp</i>	<b>LH</b>		
10	<i>LTLp</i>	<i>LTLp</i>	<i>LTLp</i>	N/A	N/A	N/A	<i>LTLp</i>	<b>LH</b>		
11	<b>LFO</b>	<i>LTLa</i>	<b>RTla</b>	<i>LTLa</i>	<i>LTLa</i>	<i>LTLa</i>	<i>LTLa</i>	<b>LFO</b>	<b>RC</b>	
12	<i>RFls</i>	<b>RFli</b>	<b>RFli</b>	N/A	N/A	N/A	<b>RP</b>			
13	<i>RFls</i>	<i>RFls</i>	<i>RFls</i>	<i>RFls</i>	<b>RCI</b>	<i>RFls</i>	<i>RFli</i>			
14	<i>RFli</i>									
15	<i>ROl</i>	<b>LTm</b>	<b>LTm</b>	<i>ROl</i>	<i>ROl</i>	<i>ROl</i>	<b>ROI</b>	<b>RPI</b>		
16	<b>RTla</b>	<b>LTm</b>	<b>LTm</b>	N/A	N/A	N/A	<b>ROI</b>	<b>RPI</b>		
17	<i>LTLa</i>	<b>LFO</b>	<b>LTm</b>	<b>LI</b>						
18	<i>LTLa</i>	<i>LTLa</i>	<i>LTLa</i>	<b>LFls</b>	<i>LTLa</i>	<i>LTLa</i>	<i>LTLa</i>	<b>LFm</b>	<b>ROF</b>	
19	<i>RTla</i>	<i>RTla</i>	<i>RTla</i>	<b>RFli</b>	<i>RTla</i>	<i>RTla</i>	<i>RTla</i>	<b>LTm</b>		

Code source maxima localizations: *italic* confirmed by iEEG, **bold** not confirmed by iEEG, **bolditalic** contralateral hemisphere compared to negative amplitude peak in EEG and zero line in MEG topography

ESI electric source imaging; MSI magnetic source imaging; iEEG intracranial EEG; iEEG I–IV regions of interest (ROIs) with recorded interictal discharges (IEDs) in iEEG; Cl central, lateral; Cm Central, mesial; Fla frontal, lateral inferior; Fls frontal, lateral superior; Fm frontal, mesial; Fo frontal, orbital; Fp frontal, polar; Ins insula; Ob occipital, basal; Ol occipital, lateral; Om occipital, mesial; Pl parietal, lateral; Pm parietal, mesial; Tb temporal, basal; Tla temporal, lateral anterior; Tlp temporal, lateral posterior; Tm temporal mesial



most often confirms MSI cMEM source maxima relative to COH and IID. Compared to COH and IID, ESI and MSI findings using cMEM had less often secondary source maxima. In addition, MSI cMEM localizations exhibited fewer sources that are in disagreement with the electric or magnetic field topography in the sensor space than COH and IID.

The methodological reasons why cMEM performs better than IID and COH when assessing the spatial extent of the underlying sources of IEDs has been discussed for MEG in details in Chowdhury et al. (2013). In the present

study, we updated these results to ESI data and we also clearly demonstrated that cMEM is less sensitive to distant, more likely spurious, secondary sources than IID and COH methods. In Chowdhury et al. (2013) we clearly demonstrated that the key idea to obtain a method able to recover the spatial extent of the source was the use of a parcellation of the whole cortical surface. As originally proposed in Amblard et al. (2004), a hidden state variable is associated to each parcel, and MEM regularization allows to switch off the parcels considered as inactive. Using extensive realistic simulations of sources of

**Fig. 5** (Study 4) Comparison of ESI and MSI results obtained with cMEM, COH and IID with iEEG clinical data in a frontal lobe epilepsy patient with focal cortical dysplasia. **A** Electric source imaging (ESI): left A1 topographic map of the averaged IEDs (red line indicates IED peak) used for ESI, right A2 ESI findings for cMEM (first row), COH (second row) and IID (third row). **B** Cortical regions of interest (ROIs) represented over the surface of a T1 MRI surface in standard space. The red lines denote boundaries between the different ROIs (from Fig. 1). ROIs within which IEDs have been found in iEEG data are red filled. **C** Magnetic source imaging (MSI): left C1 topographic map of the averaged IEDs (red line indicates IED peak) used for MSI, right C2 MSI findings for cMEM (first row), COH (second row) and IID (third row). Primary source maxima (i.e. vertex with the maximum source amplitude) are indicated with pink arrows, secondary source maxima are marked with yellow arrows for ESI and MSI. All ESI and MSI results displayed over the cortical surface are thresholded at 30 % of the maximum amplitude. ESI and MSI were performed on IEDs independently marked in EEG and MEG traces. **A2** The ESI primary source maximum was found over the right inferior frontal gyrus in all inverse solutions (more focal source localized with cMEM, overlapping with the iEEG findings). Secondary source maximum was seen only for COH and IID and involved a widespread area over the anterior aspects of the right temporal neocortical region (not covered by iEEG). **B** IEDs recorded with iEEG: lateral inferior frontal lobe **C2** MSI revealed very focal source maxima for all three methods, with their topography located inferiorly and adjacently to ESI cMEM primary source maxima. All of them are in agreement with iEEG. Secondary source maxima were seen only for COH and IID, involving bilateral mid fronto-polar regions not covered by iEEG. Because the vertex with the secondary source maximum was found over the contralateral hemisphere compared to the MEG field topography, it was counted in the group of contralateral sources (Color figure online)

**Table 3** Positive predictive values (PPVs) and sensitivities for cMEM, COH and IID for ESI and MSI to detect regions of interest (ROIs) for which IEDs were recorded by invasive EEG (iEEG)

	Inverse method	PPV	Sensitivity
MSI	cMEM	0.79	0.42
	COH	0.58	0.28
	IID	0.53	0.28
	cMEM + COH	1.00	0.25
	cMEM + IID	0.47	0.25
	COH + IID	0.44	0.22
ESI	cMEM	0.57	0.22
	COH	0.89	0.22
	IID	0.79	0.31
	cMEM + COH	0.86	0.17
	cMEM + IID	0.64	0.25
	COH + IID	0.75	0.25

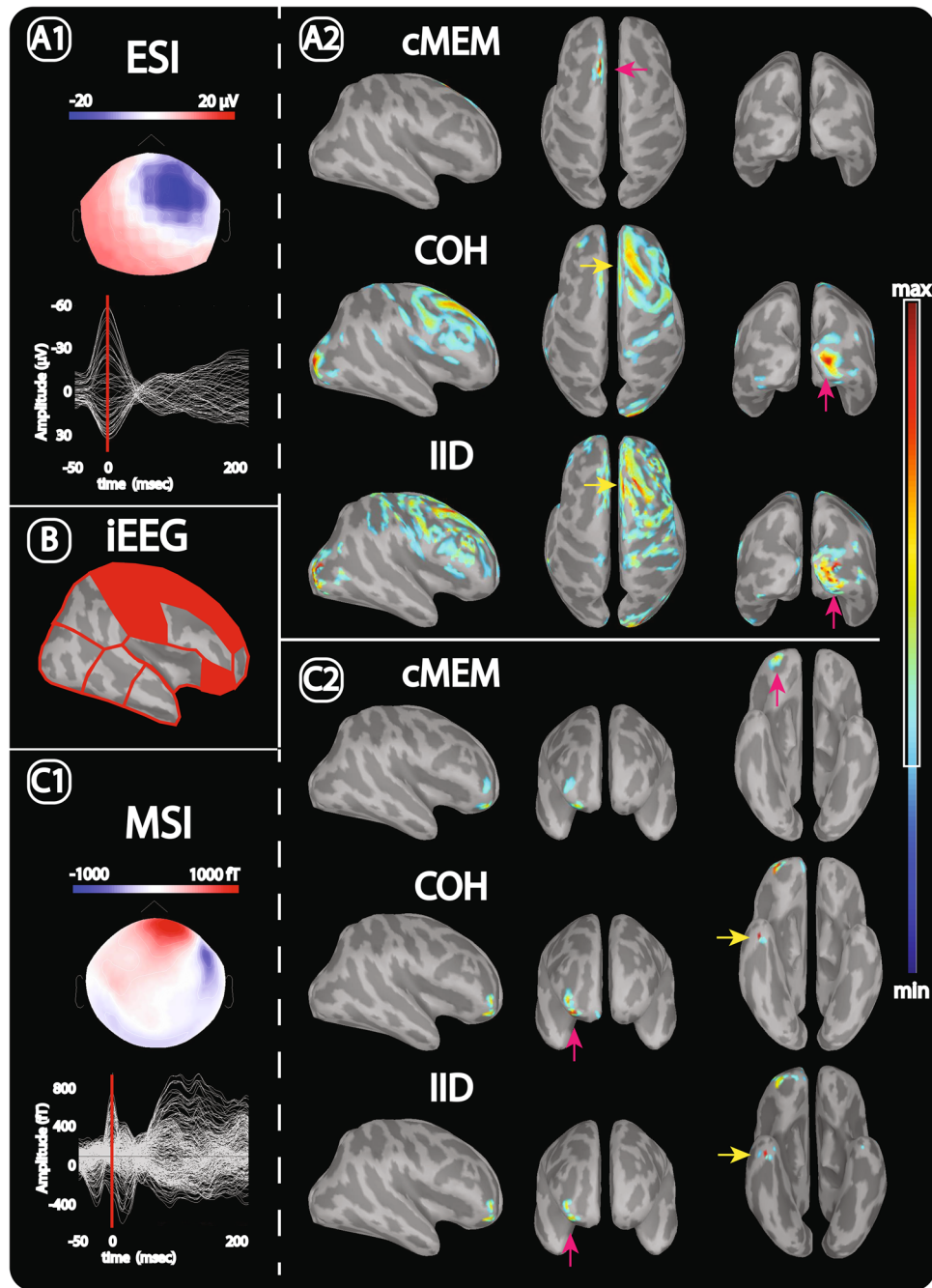
different spatial extents Chowdhury et al. (2013) demonstrated that the ability of cMEM to recover the spatial extent of the source was insensitive to the spatial scale of the parcellation. Indeed, when localizing focal sources using a model with large parcels or when localizing more

extended sources using a model with small parcels, cMEM was able to adapt by estimating an accurate contrast within the parcels considered as active, while switching off the others. Note that in this study, cMEM was also compared with an extension of COH proposed on the same parcels and we showed that for this method within the HB framework, the parcels should always be larger than the actual source extent, in order to ensure sufficient stability. Of course when dealing with real data, such an assumption is difficult to make and therefore we did not consider this extension of COH for the proposed study. IID and COH within the HB framework (Friston et al. 2008) are very similar to standard MNE and LORETA localization approaches, whereas the regularization hyperparameter was estimated from the data using Restricted Maximum Likelihood. As reported in Chowdhury et al. (2013), our present study suggests that COH combining a minimum norm and a spatial smoothness prior within HB framework is also a very interesting method to be considered when localizing IEDs. Finally we showed for the first time that cMEM seems to be quite robust to distant, more likely spurious, secondary sources, as opposed to IID and COH. This is probably associated to the ability of cMEM to switch off these more distant parcels during MEM regularization, since these generators are less likely to contribute to the recorded EEG/MEG data. IEEG recordings often confirmed source maxima for ESI with all three methods. Secondary source maxima, exclusively seen in COH and IID, were often neither confirmed by iEEG nor in agreement with the electric and magnetic field topography. Thus they are supposed to be rather spurious, although this could not be proven in the study due to limited coverage by iEEG. ESI and MSI contributed in a complementary way, with information regarding the source distribution of IEDs as described before (Heers et al. 2014).

Our simulation studies confirm the findings on clinical epilepsy data. cMEM performed equally well in simulations. cMEM ESI and MSI findings are significantly more circumscribed along the exact spatial extent of the source than those from COH and IID. Similarities between  $SD_{gs}$  and  $SD_{ngs}$  justify the use of SD without exactly known source size to assess source localization of clinical data. SD shows less spatial spread of cMEM sources for ESI and MSI compared to COH and IID in our simulations.

#### Simulations Studies of Distributed Inverse Methods

Our findings are in good agreement with those from previous simulation studies on EEG and MEG data. We have shown in a previous study that for realistic simulations of IEDs in EEG and MEG, cMEM was sensitive to the spatial



extent of the IED generators and performing well in area under the receiver operating curve (AUC) comparisons regardless their extent (median AUC value >0.8 for all spatial extents between 5 and 30  $\text{cm}^2$ ) (Chowdhury et al. 2013).

The abilities of an advanced dipole-scanning method (ExSo-MUSIC) to recover the spatial extent of the generator were evaluated in a similar framework using AUC metrics as validation (Birot et al. 2011). It performed especially well for extended sources, but less so for sources

<4  $\text{cm}^2$  (Birot et al. 2011). This may become more relevant in the near future, because there is great interest in small cortical generators of high frequency oscillations. Recently it has been reported that these small generators are detectable on the cortical surface non-invasively (Andrade-Valenca et al. 2011; von Ellenrieder et al. 2014b; Zelmann et al. 2013). Becker et al. (2014) have tested a tensor-based inverse method in realistic simulations and an example IED dataset yielding similar results as the ExSo-MUSIC algorithm.

**Fig. 6** (Study 7) Comparison of ESI and MSI results obtained with cMEM, COH and IID with iEEG clinical data, in a patient with frontal lobe epilepsy and focal cortical dysplasia. **A** Electric source imaging (ESI): left **A1** topographic map of the averaged IEDs (*red line* indicates IED peak) used for ESI, right **A2** ESI findings for cMEM (*first row*), COH (*second row*) and IID (*third row*). **B** Cortical regions of interest (ROIs) represented over the surface of a T1 MRI surface in standard space. The *red lines* denote boundaries between the different ROIs (from Fig. 1). ROIs within which IEDs have been found in iEEG data are *red filled*. **C** Magnetic source imaging (MSI): left **C1** topographic map of the averaged IEDs (*red line* indicates IED peak) used for MSI, right **C2** MSI findings for cMEM (*first row*), COH (*second row*) and IID (*third row*). Primary source maxima (i.e. vertex with the maximum source amplitude) are indicated with *pink arrows*, secondary source maxima are marked with *yellow arrows* for ESI and MSI. All ESI and MSI results displayed over the cortical surface are thresholded at 30 % of the maximum amplitude. ESI and MSI were performed on IEDs independently marked in EEG and MEG traces. **A2** ESI primary source maxima were found in the left superior frontal gyrus (cMEM) and in the right occipital pole (COH and IID). None of these locations were investigated with iEEG electrodes and the source topographies are discordant with the EEG field topography. In contrast, secondary source maxima (found only in COH and IID) were located for COH over the superior lateral frontal lobe and for IID over the mesial frontal lobe. These sources further involved a large cortical area, particularly the right dorsolateral prefrontal cortex region extending to the supplementary motor area. The COH secondary source maximum was concordant with IEDs recorded by iEEG. **B** IEDs recorded by iEEG right orbital frontal, right lateral central, right frontal lateral superior, additional IEDs recorded right hippocampus (not shown on figure) **C2** The MSI source was very focal. Source maxima were spatially concordant for the three inverse solutions, located in the right orbitofrontal region (concordant with interictal iEEG findings). Secondary source maxima were seen only for COH and IID, involving the right temporal pole (not covered by iEEG) (Color figure online)

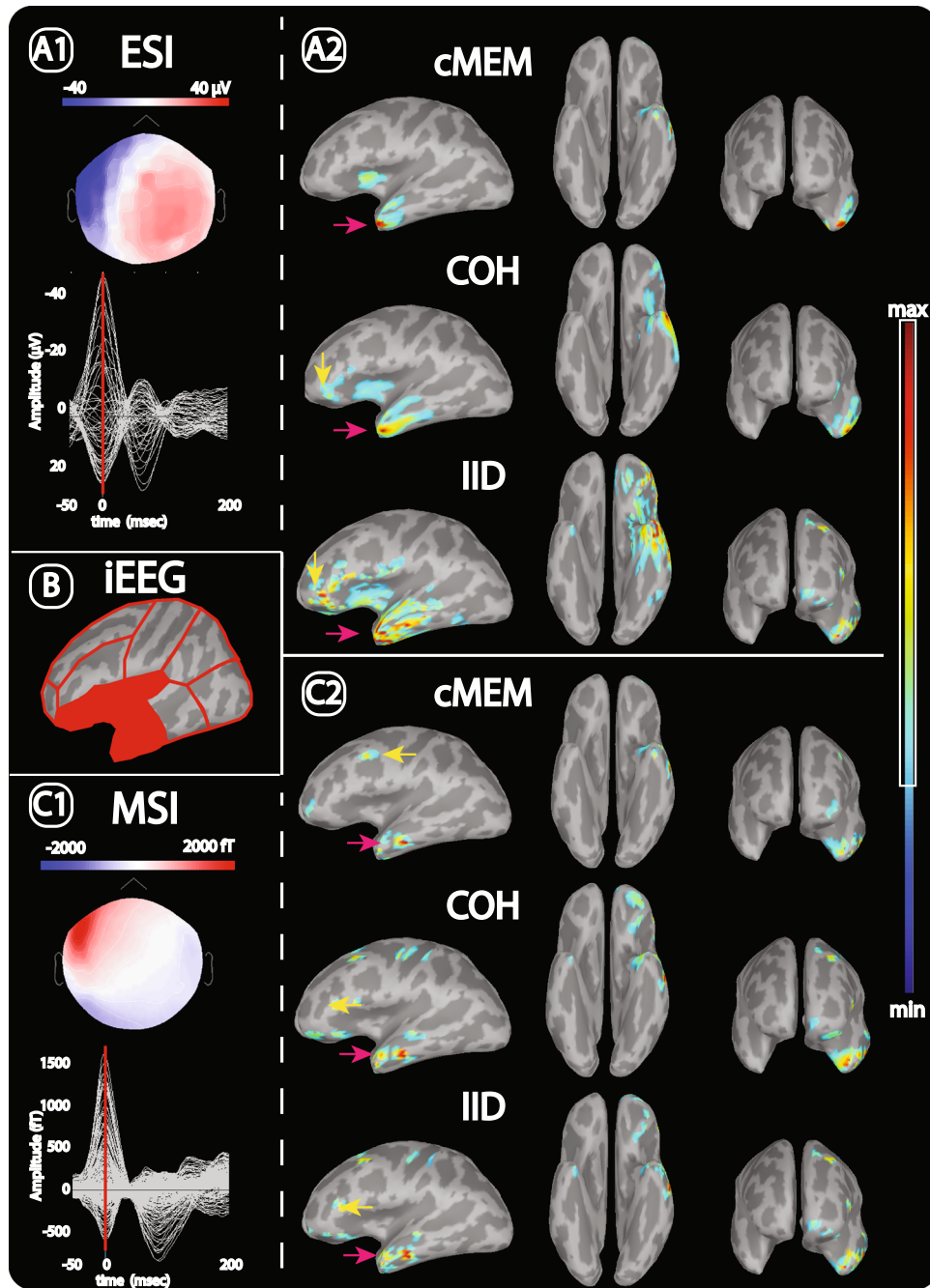
Simulations on beamforming methods showed that they suffer from several limitations: Their accuracy is highly dependent on the quality of the co-registration between sensor and MRI data (Hillebrand and Barnes 2011). This imposes a special problem for the co-registration between the MEG dewar and the patient's head, because the head is not fixed to the dewar and subsequent co-registration is a source of further error. In ESI, similar co-registration errors may occur (Dalal et al. 2014), in addition to others derived from the use of too simplistic headmodels (Steinrater et al. 2010). However, it has been shown that surface constraints would in general enable also beamformer methods to model the spatial extent of a cortical source (Hillebrand and Barnes 2011). Recently, Zhu et al. (2014) introduced a variation and wavelet based sparse source imaging (VW-SSI) method that was successfully applied on motor and language EEG/MEG data. This method was capable to accurately recover the spatial extent of the sources and to distinguish different sources better than the standard minimum norm estimation (MNE). So far VW-SSI inverse method was not applied to an epilepsy dataset (Zhu et al. 2014).

## Clinical Studies Evaluating Distributed Inverse Methods

PPVs for cMEM and COH in our study were similar to values reported before for single other MSI distributed source models alone or in combination. In the study of de Gooijer et al. all three methods used [SAM(g2), MUSIC and sLORETA] were additive. In contrast to the subdural grids comparison reported by de Gooijer-van de Groep et al. (2013), we validated our findings with depth EEG electrodes, with evidently much less cortical coverage. The different validation techniques make these two studies less comparable and the spatial under-coverage by depth electrodes is a restriction of our comparison that is based on clinical decision of the surgical strategy.

We decided to compare cMEM with two methods from the HB framework keeping in mind, that IID is a variant of MNE method and that the behavior of LORETA is very similar to that of COH, which we used in our comparison. IEDs localization using dense EEG montages have been evaluated using similar inverse methods such as LORETA (Wang et al. 2011) and sLORETA (Sohrabpour et al. 2014), as a standardized version of MNE. In these studies, ESI of IEDs have been extensively evaluated in relation to the seizure onset zone detected using subdural grids, resection volume and postsurgical outcome in small series of epilepsy patients (five pediatric patients in Sohrabpour et al. (2014), seven patients in Wang et al. (2011)). In the study of Sohrabpour et al. (2014) using high density EEG with 128 electrodes, the authors showed that localization accuracy of sLORETA findings decreased significantly when fewer electrodes were considered. The number of electrodes used did not affect, however, the extent of the sources when compared to the resection volume using ROC analysis. The localization accuracy of ESI for IEDs similarly decreased in the study of (Brodbeck et al. 2011) using less than 32 EEG electrodes compared to the use of 128–256 EEG electrodes. Thus it would be interesting to further evaluate how different numbers of channels in ESI and MSI would affect the accuracy of spatial extent estimation using cMEM source localization, whereas from our experience MNE like methods are not sensitive to the spatial extent of the sources when using either simulated data (Chowdhury et al. 2012; Grova et al. 2006) and clinical data from the present study. Because our framework was set up to evaluate surface based source-imaging results, we did not compare the results to beamformer findings that are usually evaluated in source volumes (Jung et al. 2013).

Furthermore, another promising method was evaluated on clinical data (Zhu et al. 2013). In this study, the spatial-temporal changes of the variation-based sparse cortical-



current density (VB-SCCD) was used as inverse method on real MEG IEDs. The authors report quantitative data on the accurate localization of the source and a qualitative comparison of the spatial extent better compared to MNE. Spatial dispersion evaluation of cMEM ESI/MSI findings on simulations and real data in our current study already demonstrate more objectively that cMEM is able to recover the spatial extent. Additional comparisons between cMEM, VB-SCCD and ExSo MUSIC on both simulated and clinical data would be of great interest, but was out of the

scope of the present study and will be considered in the future (Chowdhury et al. 2014).

#### ESI/MSI of IEDs Versus Source Imaging of Seizure Onset Pattern

Our study has the goal to analyze IEDs. Although IEDs frequently overlap with the seizure onset zone (Megevand et al. 2014), they may be more widely distributed. Several inverse methods have been proposed to localize notably

**Fig. 7** (Study 17) Comparison of ESI and MSI results obtained with cMEM, COH and IID with iEEG clinical data, in a patient with focal cortical dysplasia. **A** Electric source imaging (ESI): *left A1* topographic map of the averaged IEDs (*red line* indicates IED peak) used for ESI, *right A2* ESI findings for cMEM (*first row*), COH (*second row*) and IID (*third row*). **B** Cortical regions of interest (ROIs) represented over the surface of a T1 MRI surface in standard space. The *red lines* denote boundaries between the different ROIs (from Fig. 1). ROIs within which IEDs have been found in iEEG data are *red filled*. **C** Magnetic source imaging (MSI): *left C1* topographic map of the averaged IEDs (*red line* indicates IED peak) used for MSI, *right C2* MSI findings for cMEM (*first row*), COH (*second row*) and IID (*third row*). Primary source maxima (i.e. vertex with the maximum source amplitude) are indicated with *pink arrows*, secondary source maxima are marked with *yellow arrows* for ESI and MSI. All ESI and MSI results displayed over the cortical surface are thresholded at 30 % of the maximum amplitude. ESI and MSI were performed on IEDs independently marked in EEG and MEG traces. **A2** Primary ESI source maximum for cMEM, COH and IID seen in the left temporal pole was confirmed by iEEG. Secondary source maxima for COH were seen over the left inferior frontal lobe (pars orbitalis) confirmed by iEEG. The IID source maximum localized more superficial to the inferior frontal lobe. This area was not covered by iEEG. **B** iEEG recorded IEDs from the left orbitofrontal area, the left insula and the left anterior temporal lobe. **C2** MSI source maxima for the three solutions localized to the anterior aspects of the left temporal neocortex, confirmed by iEEG. Secondary MSI source maxima localized to the left dorsolateral prefrontal cortex for cMEM and in the left inferior frontal gyrus (pars triangularis) for COH and IID. The insular source maximum seen for cMEM was not rated as secondary source maximum because it did not reach the 50 % of the maximum threshold defined as minimum to be considered as secondary source maximum. In this region of interest an iEEG electrode placed within the insula recorded IEDs within the insula, so that this source would have been confirmed by iEEG (Color figure online)

oscillatory patterns occurring during epileptic seizures, as for instance combining independent component analysis with MNE (Lu et al. 2012; Yang et al. 2011). We also believe that the time–frequency implementation of cMEM method using discrete wavelet transform that we proposed in Lina et al. (2014) can be employed for this purpose and will be considered in future studies.

One restriction inherent to the analysis of epileptic seizures is that combined EEG/MEG sessions are usually only approximately one hour long, so the chances to record seizures are very low. Therefore simultaneous ESI/MSI of IEDs will remain an important contribution in the pre-surgical evaluation of epilepsy patients.

#### Limitations and Future Directions

In this retrospective study, we used remarkably less scalp EEG electrodes than MEG channels during the simultaneous EEG/MEG acquisitions (56 EEG electrodes versus 275 MEG channels). Thus, it would be interesting to know for our comparison between ESI/MSI and iEEG, whether the accuracy of ESI improves with a comparably high number of electrodes (high density EEG). Prior studies

already suggested that increasing the number of electrodes improves the localization accuracy, although the improvement seems to become less significant with more than 64 electrodes (Brodbeck et al. 2011; Lantz et al. 2003; Sohrabpour et al. 2014).

As any other study with iEEG validation, our study is limited by the spatial under-coverage in the invasive recording. In some cases, no iEEG electrodes covered the source regions, remaining unclear whether some ESI and MSI maxima could spatially correlate with IEDs, should an iEEG contact be targeting that region. Indeed, the iEEG limited spatial coverage is one of the reasons why we could not evaluate the spatial extent on iEEG data for our evaluation.

It was not the specific aim of our current study to evaluate the epileptogenic area or any relationship with resection in these patients. We intended to evaluate the performance of different inverse methods in localizing IEDs, and therefore comparing our findings with IEDs recording during iEEG, more likely to correspond to the same event detected from scalp EEG/MEG data. The originality of our proposed approach was to address IEDs localization accuracy when comparing different method, similarly to the study proposed by de Gooijer-van de Groep et al. (2013), while we believe this is the first clinical study using SD metric to assess the spatial extent of the different localization when no Gold Standard is available for that purpose. Moreover, localization of sources of IEDs should be feasible and also performed in patients that will never undergo surgery. Thus we did not compare our findings to postsurgical outcome and resection volume (Genow et al. 2004; Wang et al. 2011). Questions regarding the ability of ESI/MSI of IEDs to predict favorable post-surgical outcome should be addressed in different studies by selecting the best and most accurate inverse method determined from different studies including validation with simulation.

Additionally, as any anatomical segmentation based analysis, our ROI-based evaluation has limitations. In one example, one of the cMEM ESI (study 7) source maxima localized to the contralateral hemisphere near the interhemispheric fissure. Although this source maximum was counted in the group of contralateral sources, it was actually near the ipsilateral amplitude maximum in sensor space. Our ROI classification could not capture this detail.

Furthermore, co-registering the exact iEEG electrode positions with ESI/MSI findings would have increased the accuracy of the source imaging solutions in this study. Unfortunately, some additional methods need to be implemented, so that this kind of comparison remains out of the scope of the current work and will be investigated in another study in preparation (Grova et al. 2013). SD values of cMEM compared to COH and IID demonstrated

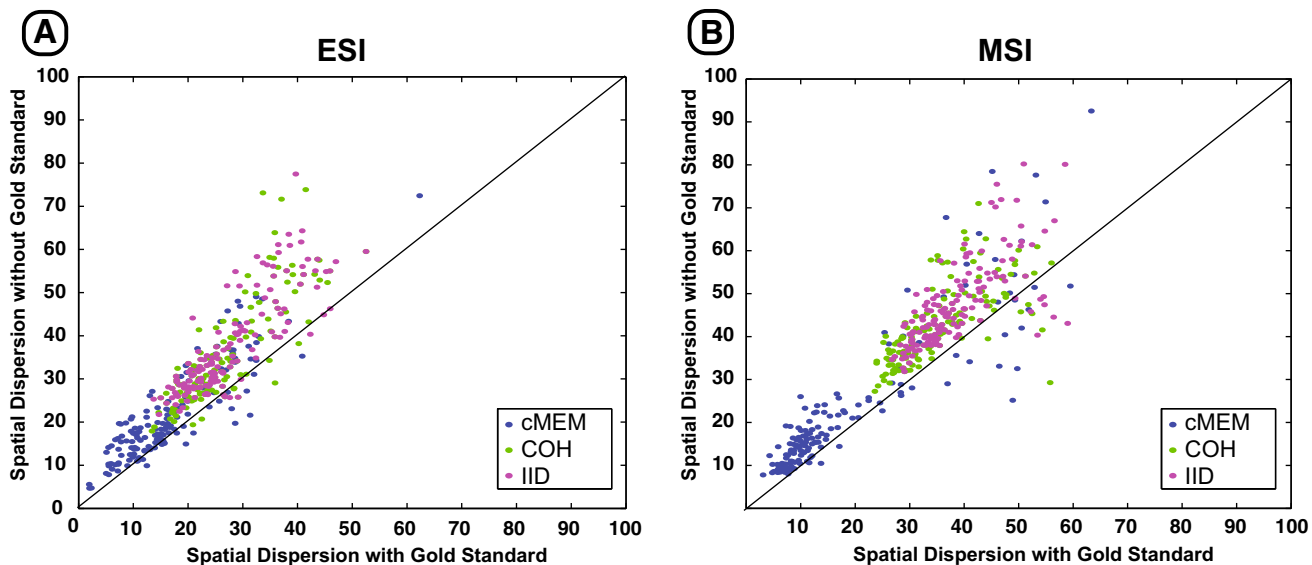


**Fig. 8** Comparison of the spatial dispersion (SD) with and without Gold Standard (i.e., gold standard = known extent localization and extent of the simulated cortical patch). The simulated cortical patches systematically varied in their extent (between 2 and 16 cm<sup>2</sup>) for ESI (A) and MSI (B). Similar results were obtained for ESI and MSI with and without Gold Standard, for different patches. Thus it justifies the

that cMEM sources are less spatially extended. In this context, cMEM sources are less likely to be spurious and are providing a more reliable representation of the underlying spatial extent of the generators. This has been confirmed in the comparison with simulated sources for ESI and MSI. The spatial extent of ESI/MSI findings should be compared with the extent of the sources on real data in patients who undergo investigation with large subdural multi-contact EEG electrodes, which is rarely done in our hospital.

## Conclusion

The performance of cMEM, COH and IID inverse solutions differs in clinical and simulated IEDs identified in simultaneous EEG/MEG data. For MSI, cMEM primary source maxima are most often confirmed by iEEG. For ESI the concordance of primary source maxima for cMEM, COH and IID with iEEG are similar between the inverse solutions. In addition, ESI/MSI cMEM sources are less often associated with secondary source maxima and are significantly less spatially spread than COH and IID sources. Because of the accurate localization of primary sources for ESI and MSI and the more accurate representation of the generator's spatial extent compared to COH and IID, our results suggest that cMEM is a valuable inverse solution to localize IEDs and should be considered in clinical applications.

use on clinical data without an exactly defined Gold Standard. This further supports assessing the spatial extent of ESI and MSI IEDs without exactly knowing the spatial extent of the sources from depth electrodes. Additionally, this figure illustrates the significantly smaller SD for cMEM compared to COH and IID, as we found it for the ESI/MSI findings from the clinical epilepsy data

**Acknowledgments** The authors thank Ms. Manon Robert for her excellent assistance in EEG/MEG data acquisition. This project was supported by the CIHR (MOP-93614), Fonds de la recherche en santé du Québec, Centres of Excellence for Commercialization and Research (CECR), American Epilepsy Society Early Career Physicians-Scientist Award and by the Savoy-Foundation. MH currently receives funding from the BrainLinks-BrainTools Cluster of Excellence funded by the German Research Foundation (DFG, grant number EXC 1086), which has not however supported any data acquisition or analysis related to the study.

**Conflict of interest** None of the authors states any conflict of interest.

## References

- Amblard C, Lapalme E, Lina JM (2004) Biomagnetic source detection by maximum entropy and graphical models. *IEEE Trans Biomed Eng* 51:427–442. doi:[10.1109/TBME.2003.820999](https://doi.org/10.1109/TBME.2003.820999)
- Andrade-Valence LP, Dubeau F, Mari F, Zelmann R, Gotman J (2011) Interictal scalp fast oscillations as a marker of the seizure onset zone. *Neurology* 77:524–531. doi:[10.1212/WNL.0b013e318228bee2](https://doi.org/10.1212/WNL.0b013e318228bee2)
- Baillet S, Mosher JC, Leahy RM (2001) Electromagnetic brain mapping. *IEEE Signal Processing Magazine* 18:14–30. doi:[10.1109/79.962275](https://doi.org/10.1109/79.962275)
- Bast T et al (2004) EEG and MEG source analysis of single and averaged interictal spikes reveals intrinsic epileptogenicity in focal cortical dysplasia. *Epilepsia* 45:621–631
- Becker H et al (2014) EEG extended source localization: tensor-based vs. conventional methods. *Neuroimage* 96:143–157. doi:[10.1016/j.neuroimage.2014.03.043](https://doi.org/10.1016/j.neuroimage.2014.03.043)
- Birot G, Albera L, Wendling F, Merlet I (2011) Localization of extended brain sources from EEG/MEG: the ExSo-MUSIC

- approach. *Neuroimage* 56:102–113. doi:[10.1016/j.neuroimage.2011.01.054](https://doi.org/10.1016/j.neuroimage.2011.01.054)
- Brodbeck V et al (2011) Electroencephalographic source imaging: a prospective study of 152 operated epileptic patients. *Brain* 134:2887–2897. doi:[10.1093/brain/awr243](https://doi.org/10.1093/brain/awr243)
- Chen F, Hallez H, Staelens S (2010) Influence of skull conductivity perturbations on EEG dipole source analysis. *Med Phys* 37:4475. doi:[10.1111/1.3466831](https://doi.org/10.1111/1.3466831)
- Chowdhury R, Zerouali Y, Lina JM, Kobayashi E, Grova C (2012) Multimodal EEG/MEG fusion within the maximum entropy on the mean (MEM) framework. In: 18th international conference on biomagnetism, BIOMAG 2012, Paris
- Chowdhury R et al (2014) Localization of the spatial extent of the generators of epileptic discharges in EEG and MEG: comparison between 4-ExSo-MUSIC and MEM approaches. In: 19th international conference on biomagnetism, BIOMAG 2014, Halifax, Canada
- Chowdhury RA, Lina J-M, Kobayashi E, Grova C (2013) MEG source localization of spatially extended generators of epileptic activity: comparing entropic and hierarchical Bayesian approaches. *PLoS One* 8:e55969. doi:[10.1371/journal.pone.0055969.s004](https://doi.org/10.1371/journal.pone.0055969.s004)
- Dalal SS, Rampp S, Willomitzer F, Ertl S (2014) Consequences of EEG electrode position error on ultimate beamformer source reconstruction performance. *Frontiers in neuroscience* 8:42. doi:[10.3389/fnins.2014.00042](https://doi.org/10.3389/fnins.2014.00042)
- de Gooijer-van de Groep KL, Leijten FSS, Ferrier CH, Huiskamp GJM (2013) Inverse modeling in magnetic source imaging: comparison of MUSIC, SAM(g2), and sLORETA to interictal intracranial EEG. *Human Brain Mapping* 34:2032–2044. doi:[10.1002/hbm.22049](https://doi.org/10.1002/hbm.22049)
- De Tiege X et al (2012) Clinical added value of magnetic source imaging in the presurgical evaluation of refractory focal epilepsy. *Journal of Neurology, Neurosurgery & Psychiatry*. doi:[10.1136/jnnp-2011-301166](https://doi.org/10.1136/jnnp-2011-301166)
- Friston KJ, Penny W, Phillips C, Kiebel S, Hinton G, Ashburner J (2002) Classical and Bayesian inference in neuroimaging: theory. *Neuroimage* 16:465–483. doi:[10.1006/nimg.2002.1090](https://doi.org/10.1006/nimg.2002.1090)
- Friston KJ et al (2008) Multiple sparse priors for the M/EEG inverse problem. *NeuroImage* 39:1104–1120. doi:[10.1016/j.neuroimage.2007.09.048](https://doi.org/10.1016/j.neuroimage.2007.09.048)
- Genow A et al (2004) Epilepsy surgery, resection volume and MSI localization in lesional frontal lobe epilepsy. *NeuroImage* 21:444–449. doi:[10.1016/j.neuroimage.2003.08.029](https://doi.org/10.1016/j.neuroimage.2003.08.029)
- Goldenholz DM, Ahlfors SP, Hämäläinen MS, Sharon D, Ishitobi M, Vaina LM, Stufflebeam SM (2009) Mapping the signal-to-noise-ratios of cortical sources in magnetoencephalography and electroencephalography. *Hum Brain Mapp* 30:1077–1086. doi:[10.1002/hbm.20571](https://doi.org/10.1002/hbm.20571)
- Goncalves SI, de Munck JC, Verbunt JPA, Bijma F, Heethaar RM, Lopes da Silva F (2003) In vivo measurement of the brain and skull resistivities using an eit-based method and realistic models for the head. *IEEE Trans Bio-med Eng* 50:754–767. doi:[10.1109/TBME.2003.812164](https://doi.org/10.1109/TBME.2003.812164)
- Gramfort A, Papadopoulou T, Olivi E, Clerc M (2010) OpenMEEG: opensource software for quasistatic bioelectromagnetics. *Bio-medical engineering online* 9:45. doi:[10.1186/1475-925X-9-45](https://doi.org/10.1186/1475-925X-9-45)
- Grova C, Daunizeau J, Lina JM, Benar CG, Benali H, Gotman J (2006) Evaluation of EEG localization methods using realistic simulations of interictal spikes. *Neuroimage* 29:734–753. doi:[10.1016/j.neuroimage.2005.08.053](https://doi.org/10.1016/j.neuroimage.2005.08.053)
- Grova C et al (2013) Evaluation of the spatial extent of the sources of epileptic spikes in MEG. In: International conference on basic and clinical multimodal imaging (BACI), Geneva, 5–8 Sept 2013
- Hämäläinen MS (1992) Magnetoencephalography: a tool for functional brain imaging. *Brain Topogr* 5:95–102
- Hämäläinen MS, Ilmoniemi RJ (1994) Interpreting magnetic fields of the brain: minimum norm estimates. *Med Biol Eng Compu* 32: 35–42
- Heers M, Hedrich T, An D, Dubois F, Gotman J, Grova C, Kobayashi E (2014) Spatial correlation of hemodynamic changes related to interictal epileptic discharges with electric and magnetic source imaging. *Hum Brain Mapp* 35:4396–4414. doi:[10.1002/hbm.22482](https://doi.org/10.1002/hbm.22482)
- Hillebrand A, Barnes GR (2011) Practical constraints on estimation of source extent with MEG beamformers. *Neuroimage* 54:2732–2740. doi:[10.1016/j.neuroimage.2010.10.036](https://doi.org/10.1016/j.neuroimage.2010.10.036)
- Iwasaki M, Pestana E, Burgess RC, Lüders HO, Shamot H, Nakasato N (2005) Detection of epileptiform activity by human interpreters: blinded comparison between electroencephalography and magnetoencephalography. *Epilepsia* 46:59–68. doi:[10.1111/j.0013-9580.2005.21104.x](https://doi.org/10.1111/j.0013-9580.2005.21104.x)
- Jung J et al (2013) The value of magnetoencephalography for seizure-onset zone localization in magnetic resonance imaging-negative partial epilepsy. *Brain* 136:3176–3186. doi:[10.1093/brain/awt213](https://doi.org/10.1093/brain/awt213)
- Knowlton RC et al (2008) Functional imaging: II. Prediction of epilepsy surgery outcome *Annals of Neurology* 64:35–41
- Kobayashi K, Yoshinaga H, Ohtsuka Y, Gotman J (2005) Dipole modeling of epileptic spikes can be accurate or misleading. *Epilepsia* 46:397–408. doi:[10.1111/j.0013-9580.2005.31404.x](https://doi.org/10.1111/j.0013-9580.2005.31404.x)
- Lantz G, Grave de Peralta R, Spinelli L, Seeck M, Michel CM (2003) Epileptic source localization with high density EEG: how many electrodes are needed? *Clin Neurophysiol* 114:63–69
- Lapalme E, Lina JM, Mattout J (2006) Data-driven parceling and entropic inference in MEG. *Neuroimage* 30:160–171. doi:[10.1016/j.neuroimage.2005.08.067](https://doi.org/10.1016/j.neuroimage.2005.08.067)
- Lina JM, Chowdhury R, Lemay E, Kobayashi E, Grova C (2014) Wavelet-based localization of oscillatory sources from magnetoencephalography data. *IEEE Trans Biomed Eng* 61:2350–2364. doi:[10.1109/TBME.2012.2189883](https://doi.org/10.1109/TBME.2012.2189883)
- Lu Y, Yang L, Worrell GA, Brinkmann B, Nelson C, He B (2012) Dynamic imaging of seizure activity in pediatric epilepsy patients. *Clin Neurophysiol* 123:2122–2129. doi:[10.1016/j.clinph.2012.04.021](https://doi.org/10.1016/j.clinph.2012.04.021)
- Mamelak AN, Lopez N, Akhtari M, Sutherling WW (2002) Magnetoencephalography-directed surgery in patients with neocortical epilepsy. *J Neurosurg* 97:865–873. doi:[10.3171/jns.2002.97.4.0865](https://doi.org/10.3171/jns.2002.97.4.0865)
- Mangin J-F, Frouin V, Bloch I, Régis J, López-Krahe J (1995) From 3D magnetic resonance images to structural representations of the cortex topography using topology preserving deformations. *Journal of Mathematical Imaging and Vision* 5:297–318. doi:[10.1007/BF01250286](https://doi.org/10.1007/BF01250286)
- Mattout J, Pelegrini-Issac M, Garnero L, Benali H (2005) Multivariate source prelocalization (MSP): use of functionally informed basis functions for better conditioning the MEG inverse problem. *Neuroimage* 26:356–373. doi:[10.1016/j.neuroimage.2005.01.026](https://doi.org/10.1016/j.neuroimage.2005.01.026)
- Megevand P et al (2014) Electric source imaging of interictal activity accurately localizes the seizure onset zone. *J Neurol Neurosurg Psychiatry* 85:38–43. doi:[10.1136/jnnp-2013-305515](https://doi.org/10.1136/jnnp-2013-305515)
- Mikuni N et al (1997) Simultaneous recording of epileptiform discharges by MEG and subdural electrodes in temporal lobe epilepsy. *NeuroImage* 5:298–306. doi:[10.1006/nimg.1997.0272](https://doi.org/10.1006/nimg.1997.0272)
- Molins A, Stufflebeam SM, Brown EN, Hamalainen MS (2008) Quantification of the benefit from integrating MEG and EEG data in minimum l2-norm estimation. *Neuroimage* 42:1069–1077. doi:[10.1016/j.neuroimage.2008.05.064](https://doi.org/10.1016/j.neuroimage.2008.05.064)
- Oishi M, Otsubo H, Kameyama S, Morota N, Masuda H, Kitayama M, Tanaka R (2002) Epileptic spikes: magnetoencephalography versus simultaneous electrocorticography. *Epilepsia* 43:1390–1395

- Pascual-Marqui RD, Michel CM, Lehmann D (1994) Low resolution electromagnetic tomography: a new method for localizing electrical activity in the brain. *Int J Psychophysiol* 18:49–65
- Rikir E et al (2014) Electrical source imaging in cortical malformation-related epilepsy: a prospective EEG-SEEG concordance study. *Epilepsia* 55:918–932. doi:[10.1111/epi.12591](https://doi.org/10.1111/epi.12591)
- Sohrabpour A, Lu Y, Kankirawatana P, Blount J, Kim H, He B (2014) Effect of EEG electrode number on epileptic source localization in pediatric patients. *Clin Neurophysiol*. doi:[10.1016/j.clinph.2014.05.038](https://doi.org/10.1016/j.clinph.2014.05.038)
- Steinrstrater O, Sillekens S, Junghofer M, Burger M, Wolters CH (2010) Sensitivity of beamformer source analysis to deficiencies in forward modeling. *Hum Brain Mapp* 31:1907–1927. doi:[10.1002/hbm.20986](https://doi.org/10.1002/hbm.20986)
- Sutherling WW, Mamelak AN, Thyerlei D, Maleeva T, Minazad Y, Philpott L, Lopez N (2008) Influence of magnetic source imaging for planning intracranial EEG in epilepsy. *Neurology* 71:990–996. doi:[10.1212/01.wnl.0000326591.29858.1a](https://doi.org/10.1212/01.wnl.0000326591.29858.1a)
- Tadel F, Baillet S, Mosher JC, Pantazis D, Leahy RM (2011) Brainstorm: a user-friendly application for MEG/EEG analysis. *Comput Intell Neurosci* 2011:879716. doi:[10.1155/2011/879716](https://doi.org/10.1155/2011/879716)
- Tao JX, Ray A, Hawes-Ebersole S, Ebersole JS (2005) Intracranial EEG substrates of scalp EEG interictal spikes. *Epilepsia* 46:669–676. doi:[10.1111/j.1528-1167.2005.11404.x](https://doi.org/10.1111/j.1528-1167.2005.11404.x)
- von Ellenrieder N, Beltrachini L, Muravchik CH, Gotman J (2014a) Extent of cortical generators visible on the scalp: effect of a subdural grid. *Neuroimage*. doi:[10.1016/j.neuroimage.2014.08.009](https://doi.org/10.1016/j.neuroimage.2014.08.009)
- von Ellenrieder N, Beltrachini L, Perucca P, Gotman J (2014b) Size of cortical generators of epileptic interictal events and visibility on scalp EEG. *Neuroimage* 94:47–54. doi:[10.1016/j.neuroimage.2014.02.032](https://doi.org/10.1016/j.neuroimage.2014.02.032)
- Wang G, Worrell G, Yang L, Wilke C, He B (2011) Interictal spike analysis of high-density EEG in patients with partial epilepsy. *Clin Neurophysiol* 122:1098–1105. doi:[10.1016/j.clinph.2010.10.043](https://doi.org/10.1016/j.clinph.2010.10.043)
- Wennberg R, Cheyne D (2014a) EEG source imaging of anterior temporal lobe spikes: validity and reliability. *Clin Neurophysiol* 125:886–902. doi:[10.1016/j.clinph.2013.09.042](https://doi.org/10.1016/j.clinph.2013.09.042)
- Wennberg R, Cheyne D (2014b) Reliability of MEG source imaging of anterior temporal spikes: analysis of an intracranially characterized spike focus. *Clin Neurophysiol* 125:903–918. doi:[10.1016/j.clinph.2013.08.032](https://doi.org/10.1016/j.clinph.2013.08.032)
- Yang L, Wilke C, Brinkmann B, Worrell GA, He B (2011) Dynamic imaging of ictal oscillations using non-invasive high-resolution EEG. *Neuroimage* 56:1908–1917. doi:[10.1016/j.neuroimage.2011.03.043](https://doi.org/10.1016/j.neuroimage.2011.03.043)
- Zelmann R, Lina JM, Schulze-Bonhage A, Gotman J, Jacobs J (2013) Scalp EEG is not a blur: it can see high frequency oscillations although their generators are small. *Brain Topogr*. doi:[10.1007/s10548-013-0321-y](https://doi.org/10.1007/s10548-013-0321-y)
- Zhu M, Zhang W, Dickens DL, King JA, Ding L (2013) Sparse MEG source imaging for reconstructing dynamic sources of interictal spikes in partial epilepsy. *J Clin Neurophysiol* 30:313–328. doi:[10.1097/WNP.0b013e31829dda27](https://doi.org/10.1097/WNP.0b013e31829dda27)
- Zhu M, Zhang W, Dickens DL, Ding L (2014) Reconstructing spatially extended brain sources via enforcing multiple transform sparseness. *Neuroimage* 86:280–293. doi:[10.1016/j.neuroimage.2013.09.070](https://doi.org/10.1016/j.neuroimage.2013.09.070)